# Photochromic Behavior in the Fluorescence Spectra of 9-Anthrol Encapsulated in Si−Al Glasses Prepared by the Sol−Gel Method

**Tsuneo Fujii,* Kazuhiko Kodaira, Osamu Kawauchi, and Nobuaki Tanaka**

*Department of Chemistry and Materials Engineering, Faculty of Engineering, Shinshu University, Wakasato, Nagano 380, Japan*

**Hiromi Yamashita and Masakazu Anpo**

*Department of Applied Chemistry, College of Engineering, Osaka Prefecture University, Sakai, Osaka 593, Japan*

*Received: May 7, 1997; In Final Form: September 4, 1997*[⊗]

The fluorescence spectra of 9-anthrol during the sol−gel−xerogel transitions of 13 systems containing different silicon and aluminum ratios and catalysts have been observed at a constant temperature (300 K) as a function of the sol−gel reaction time. Fluorescence decay curves for typical xerogel samples also have been observed. 9-Anthrol in the sol−gel systems showed four different fluorescence bands originating from the hydrogen-bonded, the complex, the ion pair, and the anion form species. Continuous light irradiation of the xerogels at 360 nm led to an increase in the fluorescence at 480 nm. These findings indicate that anthrone transforms to 9-anthrol by the photoinduced intermolecular proton transfer in these matrixes. The most effective and remarkable tautomerization occurred in the Si:Al = 90:10 system, and it was concluded that this photochromic behavior occurs by the photoinduced proton transfer from a proton at the surface Brønsted acid site on the −O−Si−O−Al−O− network to the anthrone molecule.

## Introduction

Photochromism of organic compounds in heterogeneous systems is a phenomenon with great potential not only for practical applications but also for elucidating primary photochemical reactions.[1−9] The photophysical processes of aromatic carbonyl molecules in solutions and solid matrixes depend on the geometrical and electronic properties of the individual molecules as well as on the physicochemical properties of the surrounding matrixes.[10,11] The characteristic changes observed in the molecules have been substantially explained by the close proximity of the n−$\pi$* and $\pi$−$\pi$* levels of both the singlet and triplet states. However, keto−enol tautomerization in aromatic carbonyl compounds complicates the situation. Hydroxyanthraquinones show the formation of intramolecular hydrogen-bonding or the intramolecular excited-state proton transfer between the keto and enol forms.[12−16] Molecules characterized by the capacity for excited-state proton transfer are of great interest in connection with photochemical hole burning.[3,17−19] Nonfluorescent anthrone is known to become a fluorescent molecule through the keto−enol tautomerization to 9-anthrol (see Scheme 1).[20−24] In this work, we have investigated the fluorescence spectra of 9-anthrol during the sol−gel−xerogel transitions of 13 systems containing silicon and aluminum alkoxides in different ratios, (Si:Al = 100:0, 99:1, 90:10, 80:20, 70:30, 60:40, and 50:50) in heterogeneous systems using small amounts of HCl or NaOH as the catalyst at a constant temperature (300 K), as a function of the sol−gel reaction time.[25−33] The fluorescence lifetimes of typical xerogels have also been measured. It was found that anthrone molecules encapsulated into the xerogels show photochromic behavior in the fluorescence spectra originating from the photoinduced proton transfer between anthrone and a proton at the surface Brønsted acid site existing on the −O−Si−O−Al−O− network.

**SCHEME 1: Keto−Enol Equilibrium between Anthrone and 9-Anthrol**

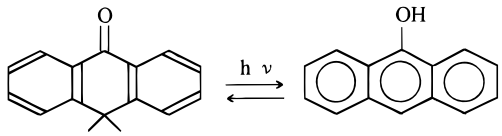


## Experimental Section

Anthrone (Wako JIS first grade) was purified by repeated recrystallization from acetic acid and an ethanol−water mixture. Methanol, ethanol, TEA (triethylamine), HCl and NaOH supplied by Wako (Luminasol, Spectrosol, JIS S, or JIS reagent grade), TEOS (tetraethyl orthosilicate) from Shin-Etsu Chemicals Co. Ltd., and SAE (diisobutoxyaluminum triethylsilane $[(OBu^i)_2-Al-O-Si-(OEt)_3]$) from Dynamit Nobel were used without further purification. Water was deionized and distilled.

A $5 \times 10^{-4}$ M (M = mol dm$^{-3}$) solution of anthrone (9-anthrol) in ethanol was prepared. The starting solutions of the reaction systems contained 10.0 cm$^3$ of the anthrone solution, 10 cm$^3$ mixtures of TEOS and SAE, and 0.2 cm$^3$ of a $1.0 \times 10^{-4}$ M HCl or NaOH aqueous solution for the A and B system series (see below), except for systems A-0 and B-0 where 3.4 cm$^3$ of a $1.0 \times 10^{-4}$ M HCl or NaOH aqueous solution was used. The solutions were stirred during the gradual mixture of the starting compounds, then stirred thoroughly for a further 5 min and the total volumes were adjusted to 20.2 cm$^3$. A 3 cm$^3$ aliquot of the mixed solutions was poured into individual plastic cells. The procedures were all carried out under a nitrogen atmosphere. The molar ratios of Si: Al were 100:0, 99:1, 90:10, 80:20, 70:30, 60:40, and 50:50 for the systems, abbreviated as systems A-0, A-1 ... and A-50, etc., for HCl catalysts and B-1, B-30, etc., for the NaOH catalysts, respectively. The acid and basic solutions refer to ca. 0.1 cm$^3$ of the 0.1 M HCl or NaOH aqueous solution added to the 10 cm$^3$ ethanol solution of anthrone (9-anthrol), respectively.

[⊗] Abstract published in *Advance ACS Abstracts,* November 15, 1997.

S1089-5647(97)01540-X CCC: $14.00 

The cells were covered with a thin film with three pinholes and allowed to undergo a sol−gel−xerogel reaction at 300 K under dark conditions. The emission spectra were observed using a Shimadzu RF-5000 fluorescence spectrometer by the surface-emission method at room temperature. In the photochromic experiments, the gels were set for more than 120 days after preparing the starting solution. The relative fluorescence intensity at the starting point of the photochromic observation was adjusted using the fluorescence intensity of anthracene in cyclohexane ($1.0 \times 10^{-4}$ M). The time variation of the fluorescence intensity at 480 nm with continuous irradiation of light at 360 nm was observed every 10 s. The data were transferred to an NEC PC-9801 personal computer for processing.

The fluorescence decay curves for the A-0, A-1, A-10, A-20, and A-50 xerogel systems were measured using a Hamamatsu C-4334 streak scope with an $N_2$ dye laser. The fluorescence decay curves of 9-anthrol encapsulated in the xerogels cannot be represented by a single exponential and can be well described by eq 1,

$$I(t) = A_1 \exp(-t/\tau_1) + A_2 \exp(-t/\tau_2) \quad (1)$$

The average lifetime, $\bar{\tau}$, relative fluorescence quantum yields, $\varphi_1^r$ and $\varphi_2^r$, could be calculated from eqs 2 and 3.[24−36]

$$\bar{\tau} = \frac{A_1\tau_1^2 + A_2\tau_2^2}{A_1\tau_1 + A_2\tau_2} \quad (2)$$

$$\varphi_1^r = A_1\tau_1/(A_1\tau_1 + A_2\tau_2) \quad (3a)$$

$$\varphi_2^r = A_2\tau_2/(A_1\tau_1 + A_2\tau_2) \quad (3b)$$

Front-face excitation and observation was performed for the fluorescence, excitation, and fluorescence decay measurements.

## Results and Discussion

**Characteristics of the Four Fluorescence Bands and Excitation Spectra of 9-Anthrol in Solution.**[24] 9-Anthrol in solution shows five characteristic fluorescence bands depending on the polarity and character of the matrixes and the extent of the interaction with the surrounding environment. The characteristics of the existing species may serve as reference spectra for elucidating the fluorescence properties of 9-anthrol during the sol−gel reaction. Although, anthrone is not a fluorescent molecule, keto−enol tautomerization from anthrone to 9-anthrol is responsible for the appearance of the fluorescence. Figure 1a shows the fluorescence spectra of 9-anthrol in the various solutions. The peak wavelengths ($\lambda_{F,\,max}$) locate at 442, 454, 472, 539, and 550 nm in benzene, methanol, SAE, TEA, and the basic solutions, respectively. The fluorescence-excitation spectra of 9-anthrol in the various solvents are shown in Figure 1b. It can be seen that the spectra observed in benzene and methanol are characterized by vibrational peaks at 367, 385, and 405 nm and a shoulder at around 350 nm. The spectra observed in TEA and SAE shift to the red and their peaks are located at 388 and 399 nm, respectively. The spectrum observed in the basic solvent is characterized by two bands which are seen at around 360 and 450 nm.

Taking into account the dipole moment in the ground-state calculated by PM3 MO and the excitation energies by CNDO/S calculations, in addition to the absorption, fluorescence, and fluorescence-excitation spectra of 9-anthrol in the various solvents, the absorption bands observed was found to originate from the neutral (benzene), the hydrogen-bonded neutral (methanol, ethanol and acidic solvent), the complex (SAE, TEA, and $H_2O$), and the anion (basic solvent) species in the ground state as well as the neutral (benzene, $\lambda_{F,\,max} = 442$ nm), the hydrogen-bonded neutral (methanol, ethanol and acidic solvent, $\lambda_{F,\,max} = 454$ nm), the complex (SAE, $\lambda_{F,\,max} = 472$ nm), the ion-pair (TEA and $H_2O$, $\lambda_{F,\,max} = 539$ nm), and the anion (basic solvent, $\lambda_{F,\,max} = 550$ nm) species in the fluorescent state.

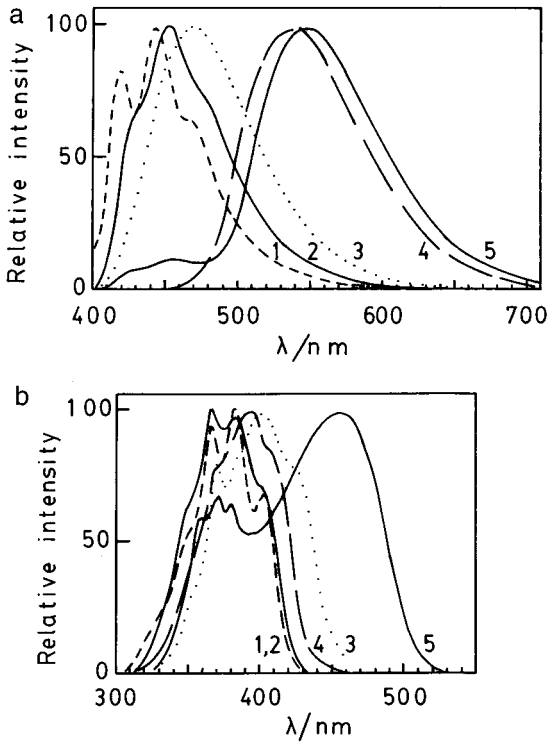


**Figure 1.** (a) Fluorescence spectra of 9-anthrol ($10^{-5}$ M) in (1) benzene, (2) methanol, (3) SAE, (4) triethylamine, and (5) the basic solution excited at 368 nm. (b) Fluorescence−excitation spectra of 9-anthrol ($10^{-5}$ M) in (1) benzene, (2) methanol, (3) SAE, (4) triethylamine, and (5) the basic solution monitored at 480 nm for (1) to (4) and 550 nm for (5).

**Fluorescence and Excitation Spectra during the Sol−Gel−Xerogel Transitions.** The fluorescence spectra of 9-anthrol during the sol−gel−xerogel transitions of the reaction systems can be characterized by the Si-to-Al ratio of the reaction systems. Figure 2a shows the typical fluorescence spectra of 9-anthrol during the sol−gel−xerogel transition of sample A-0 as a function of time. Just after mixing, the spectrum showed a peak at 450 nm corresponding to the hydrogen-bonded neutral species. The spectrum observed at 2 days was essentially the same as that observed on the first day, though the fluorescence intensity was weaker and the vibrational structure became clearer. A broad fluorescence spectrum was observed at 5 days. Gelation was observed at 6 days and the spectrum which shifted to the red peaked at 472 nm indicating the existence of a complex in the sample. At 67 days, the peak shifted to 478 nm and the contribution at around 500 nm increased. It should be noted that the fluorescence intensity was restored after the gelation point. This indicates that the amount of 9-anthrol obtained just after mixing the solution decreased after 2 days and was restored after reaching the gelation point.

Figure 2b shows the peak wavelength changes of fluorescence spectra for samples A-0 (○), A-20 (△), and A-50 (□) together with B-0 (●) and B-50 (■) and indicates that the change in the main fluorescent species can be explained by a single manner. In sample A-20, gelation was observed at 2 days. Just after mixing the solution, the peak wavelength located at 454 nm corresponding to the hydrogen-bonded neutral species. The influence of Al inclusion was not obvious at this stage. During the first stage of the reaction, the peak wavelength shifted to the blue in accordance with the progress of the sol−gel reaction.

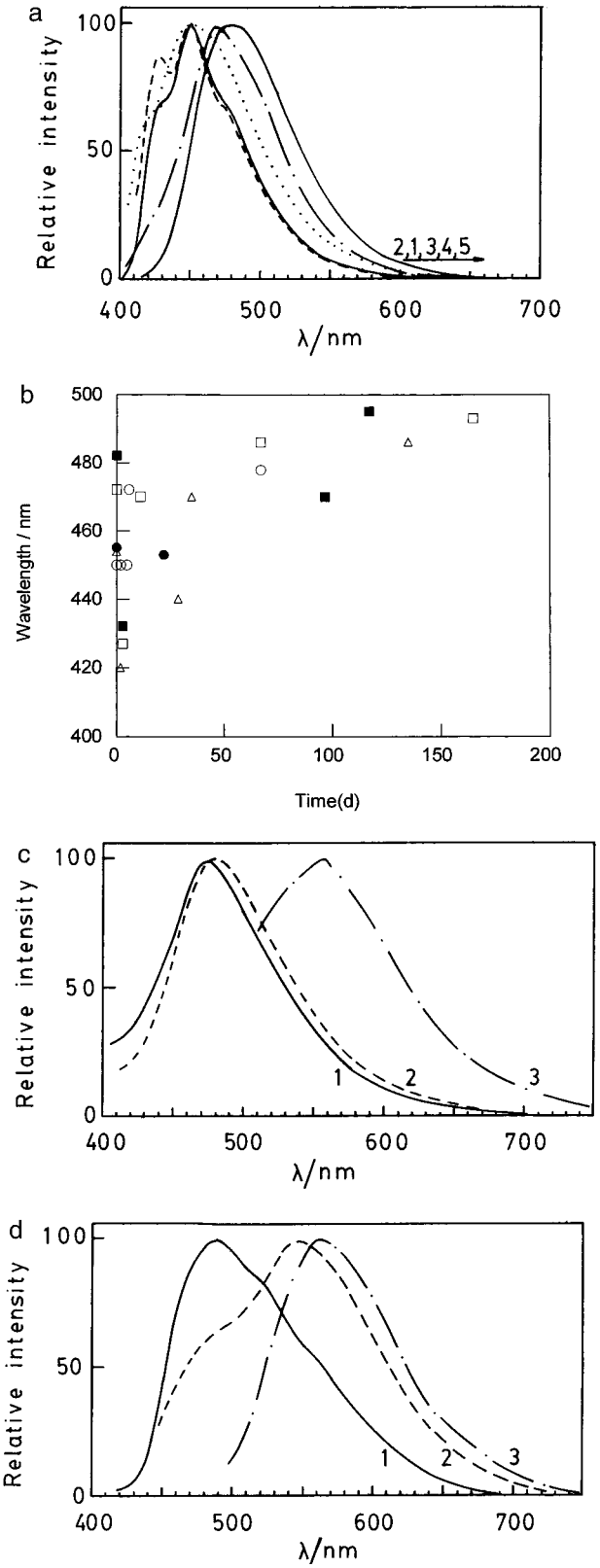


**Figure 2.** (a) Fluorescence spectra of 9-anthrol excited at 368 nm during the sol−gel−xerogel transition for sample A-0. (b) Peak wavelength changes of the fluorescence spectra of 9-anthrol for samples A-0 (○), A-20 (△), A-50 (□), B-0 (●), and B-50 (■). Fluorescent forms of 9-anthrol are indicated. Excitation wavelength dependence of the fluorescence spectra for (c) sample A-1 at 67 days and (d) sample A-50 at 165 days. Excitation wavelength: 1, 368 nm; 2, 420 nm; and 3, 470 nm.

The fluorescence intensity became weak compared with that observed on the first day while the spectrum became broad. This spectrum could not be observed in Figures 1 and 2a. At 35 days, however, the fluorescence peak observed at 470 nm, indicated the existence of a complex fluorescence originating from the interaction between 9-anthrol and the Al atoms in the gel network. The spectrum at 134 days showed the peak wavelength at 486 nm and the contribution at around 550 nm can be explained by the increased anionic species.

Gelation was observed at 3 days for sample A-50. Just after mixing, the spectrum showed a peak at 472 nm corresponding to the complex species. The spectrum observed at 3 days, however, shifted to the blue and the fluorescence intensity became weak compared with that observed on the first day while the spectrum became broad. Since no corresponding spectra can be seen in Figures 1 and 2a, the origin of the spectrum observed at 3 days is not clear as can be seen in the previous Figures. At 11 days the spectrum shifted to the red. At 67 days, the peak which was assigned to the spectrum of the complex shifted to 486 nm while the contribution from the ion pair species at around 540 nm increased.

The excitation wavelength dependence of the fluorescence spectra for samples A-1 at 67 days and A-50 at 165 days are shown in Figure 2, c and d, respectively. Four main fluorescence bands can be observed and their peak wavelengths correspond to the hydrogen-bonded, complex, ion-pair, and anion forms. It was noted that the fluorescence peaks for the hydrogen-bonded, complex, ion-pair, and anion forms in the xerogels were located at around 455, 480, 540, and 560 nm, respectively.

The typical fluorescence excitation spectra of 9-anthrol monitored at 480 nm during the sol−gel−xerogel transitions of samples A-0, A-20, and A-50 are shown in Figure 3, a, b, and c, respectively. The excitation spectra observed just after starting the A-0 and A-20 reaction systems are characterized by a peak at 386 nm showing the hydrogen-bonding species in the ground state. The spectral change in the A-0 system during the reaction was small and at 82 days the peak wavelength was located at 396 nm, almost the same as was observed for SAE, indicating the formation of a complex with the surrounding matrix. The spectrum observed in the A-20 system showed a broad feature at 134 days and peaked at 398 nm. The excitation spectra observed just after starting the A-50 reaction system was characterized by a peak at 400 nm showing that 9-anthrol forms a complex with the surrounding matrix in the ground state. The contribution from the anionic species at around 436 nm in the A-50 system could be observed at 165 days.

The monitored wavelength dependence of the fluorescence excitation spectra for samples A-1 at 67 days and A-50 at 165 days are shown in Figure 3, d and e, respectively. Four main absorption bands can be seen and their peak wavelengths correspond to the hydrogen-bonded, complex, ion-pair, and anion forms. It was noted that the fluorescence excitation peaks for the hydrogen-bonded, the complex, the ion-pair, and the anion form species in the xerogels are located at around 380, 398, 436, and 465 nm, respectively.

Although the fluorescence and excitation spectra in the basic-catalyzed reaction systems have somewhat larger contributions from the anionic species, the spectral characteristics for systems A-1, A-10, A-30, A-40, B-1, B-10, B-20, B-30, B-40, and B-50 essentially show intermediate properties in their fluorescence and excitation spectra among systems A-0, A-20, and A-50. Taking into account the results shown in Figures 2 and 3, the contribution from the complex species increased when the Al content among the samples increased.

**Fluorescence Lifetimes of 9-Anthrol Encapsulated in Si−Al Binary Oxide Xerogels.** Typical fluorescence decay curves of 9-anthrol encapsulated in A-10 and A-50 xerogels are shown in Figure 4. The deconvolution was performed by assuming a double-exponential decay as in eq 1 and the results indicate a

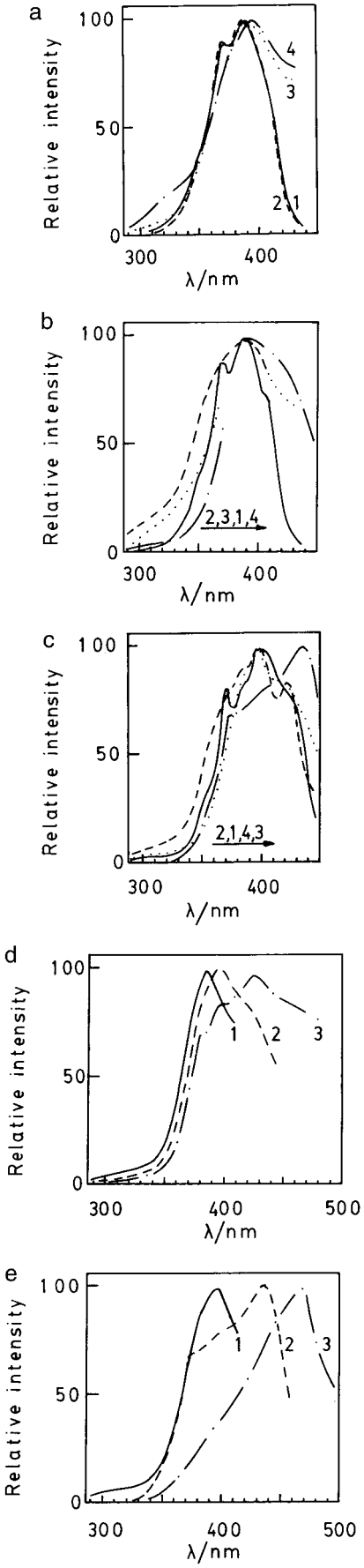


**Figure 3.** Fluorescence excitation spectra of 9-anthrol during the sol−gel−xerogel transitions: (a) sample A-0, (b) sample A-20, and (c) sample A-50. Monitored wavelength dependence of fluorescence excitation spectra of 9-anthrol during the sol−gel−xerogel transitions: (d) sample A-1 at 67 days and (e) sample A-50 at 165 days. Monitored wavelength: 1, 432 nm (d) or 450 nm (e); 2, 480 nm; 3, 560 nm.

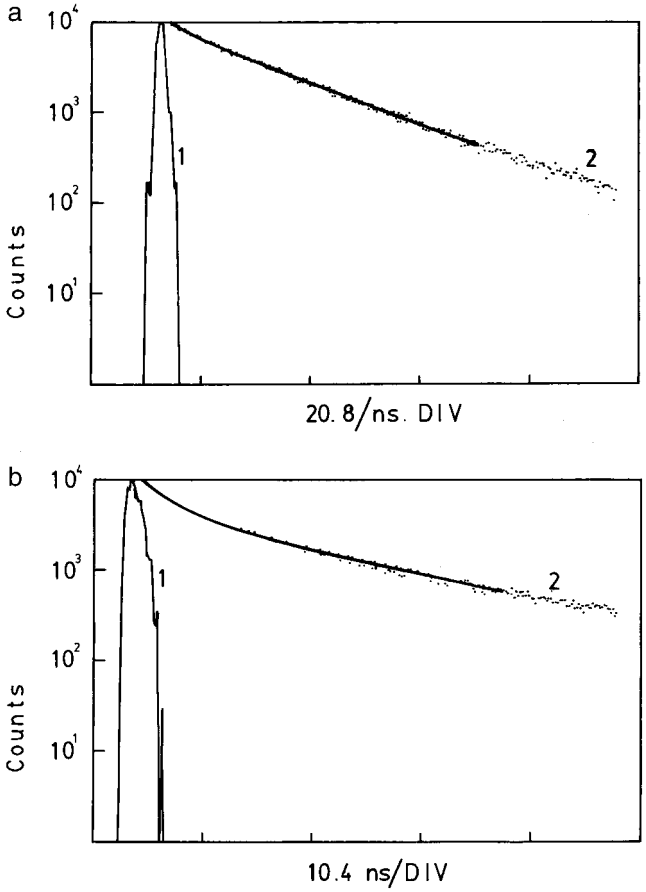


**Figure 4.** Fluorescence decay curve of 9-anthrol encapsulated in sample A-10 (a) and A-50 (b): 1, excitation pulse profile; 2, decay curve monitored at 480 nm.

**TABLE 1: Fluorescence Lifetimes ($\tau$), Their Coefficients, Average Lifetime ($\bar{\tau}$), and Relative Fluorescence Quantum Yields ($\varphi_1^r$ and $\varphi_2^r$) of 9-Anthrol in Various Gels[a]**

| Si:Al | $\tau_1$ (ns) | $\tau_2$ (ns) | $A_1$ | $A_2$ | $\bar{\tau}$ (ns) | $\varphi_1^r$ | $\varphi_2^r$ |
|---|---|---|---|---|---|---|---|
| 100:0 | 7.0 | 16.7 | 0.023 | 0.005 | 10.3 | 0.66 | 0.34 |
| 99:1 | 5.5 | 18.8 | 0.017 | 0.062 | 17.8 | 0.07 | 0.93 |
| 90:10 | 4.0 | 19.6 | 0.024 | 0.103 | 18.9 | 0.05 | 0.95 |
| 80:20 | 3.3 | 18.7 | 0.019 | 0.065 | 18.0 | 0.05 | 0.95 |
| 50:50 | 3.6 | 17.1 | 0.049 | 0.031 | 13.7 | 0.25 | 0.75 |

[a] Excitation wavelength: 337 nm, monitored at 480 nm, at 295 K.

good coincidence. The data determined by this method, the average lifetime, $\bar{\tau}$, and relative fluorescence quantum yields, $\varphi_1^r$, and $\varphi_2^r$, by eqs 2 and 3 are given in Table 1. The long and short lifetimes are ca. 5 and ca. 18 ns, respectively. Table 1 shows that the values of $\varphi_1^r$ were determined as 0.66, 0.07, and 0.25 in the A-0, A-10, and A-50 systems, respectively. However, the values of $\varphi_2^r$ from the A-0 to A-10 systems rapidly increases from 0.34 to 0.93 by adding Al atoms to the pure Si system. Therefore, the short and long fluorescence lifetimes correspond to the hydrogen-bonded and complex fluorescences, respectively. $\varphi_2^r$, the relative fluorescence quantum yield from the complex species, is dominant in all Al containing systems. The contribution from $\varphi_2^r$ decreases from 0.95 to 0.75 with an increase in Al content from the A-20 to A-50 systems indicating a change in the capacity for complex formation in these matrixes. The average lifetime, $\bar{\tau}$, is sensitive on the molecular environment and therefore this value can be used to characterize the physicochemical properties of the matrixes.[35−37] $\bar{\tau}$ value becomes the maximum at Si: Al = 90: 10 system. Based on the results shown in Figures 2 and 3, we

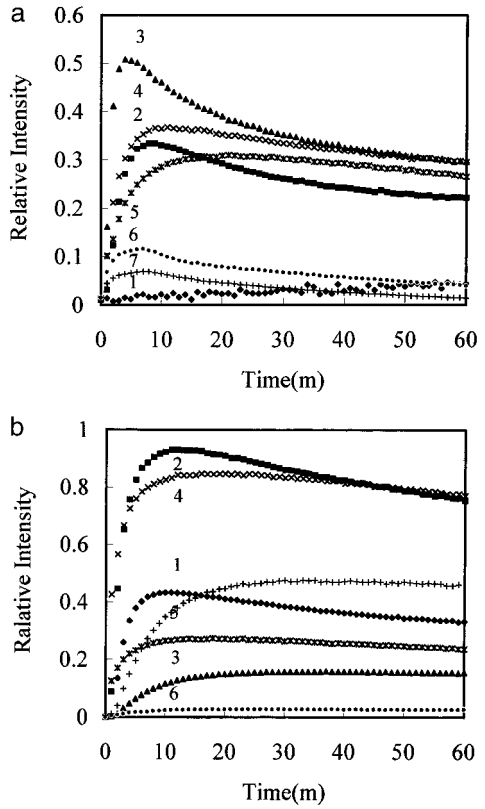


**Figure 5.** Change in the fluorescence intensity of 9-anthrol at 480 nm by 360 nm excitation. (a) 1−7: A-0, A-1, A-10, A-20, A-30, A-40, and A-50; (b) 1−6: B-1, B-10, B-20, B-30, B-40, and B-50.

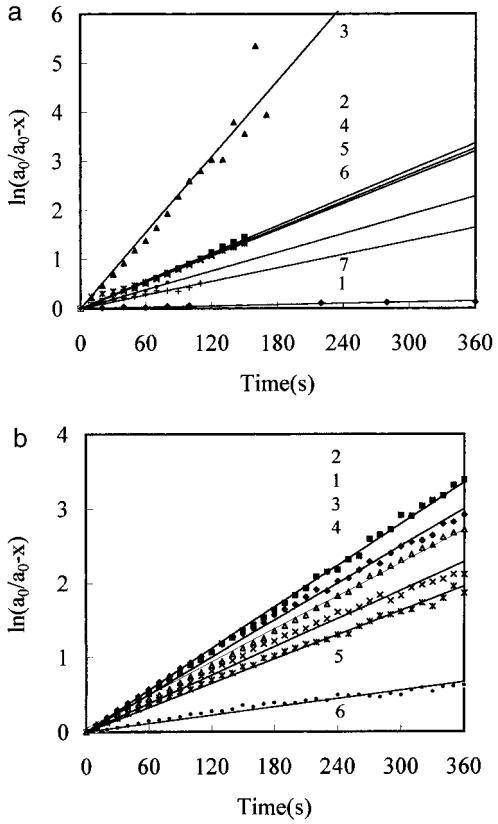


**Figure 6.** First-order plot of $\ln[a_0/(a_0 - x)]$ versus time. (a) 1−7: A-0, A-1, A-10, A-20, A-30, A-40, and A-50; (b) 1−6: B-1, B-10, B-20, B-30, B-40, and B-50.

have found substantial evidence indicating the contributions from the complex species are dominant in the Al-containing samples.

**Photochromic Behavior in the Fluorescence Spectra of 9-Anthrol Encapsulated in the Xerogels.** Photochromism in restrained systems is an attractive field with much potential.[3,4] We found that continuous irradiation of light at 360 nm on the xerogel systems including anthrone and/or 9-anthrol changes the fluorescence intensity at around 480 nm fluorescence (mainly composed of the contribution from the complex fluorescence). The relative intensity changes at 480 nm for the A- and B-systems, $I_{(480\ nm)}$, vs the irradiation time are shown in Figure 5. All systems showed that after $I_{(480\ nm)}$ reached a maximum, they decreased in intensity. The interchange between the fluorescent species at ca. 480 nm is responsible for the increase and the decrease in $I_{(480\ nm)}$. Just after the start of irradiation, the fluorescence intensity was found to increase rapidly as a function of time. This increase is believed to be due to the change in chemical species by a photoinduced proton transfer from anthrone to 9-anthrol. On the other hand, after the intensity peaks, the formation of the anionic species and/or nonfluorescent species can be said to be responsible for the decrease in the fluorescence intensity at ca. 480 nm.

First-order plots[37] during the initial period of irradiation for the systems A and B are shown in Figure 6. Clear linear relationships can be seen for the systems indicating that a first-order photoinduced proton transfer reaction occurs in the systems. These results suggest that the rise in time is directly proportional to the residual concentration of anthrone. Figure 7 plots the obtained first-order reaction constant, $k$, and $I_{max}/I_0$ vs Al/(Si + Al) for systems A and B. It was noted that $k$ shows the maximum value in the A-10 and B-10 systems, while the order of $k$ was found to be A-10 > A-20 ∼ A-1 > A-30 > A-40 > A-50 > A-0 and B-10 > B-1 > B-20 > B-30 > B-40 > B-50. This order for systems A and B agrees well with the

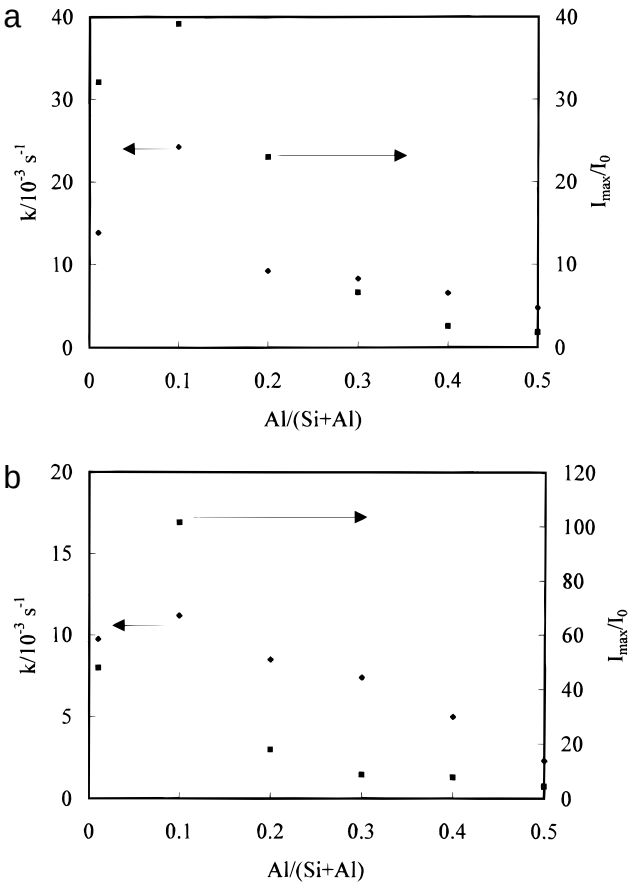


**Figure 7.** Relations between $k$ vs Al/(Si + Al) and $I_{max}/I_0$ vs Al/(Si + Al) for the samples A (a) and B (b).

results of $I_{max}/I_0$ vs Al/(Si + Al) and also with the finding that the $\bar{\tau}$ value reaches a maximum at the system of Si:Al = 90:10.

**SCHEME 2: Mechanism of Photoinduced Intermolecular Proton Transfer between Anthrone and 9-Anthrol in the Pores**

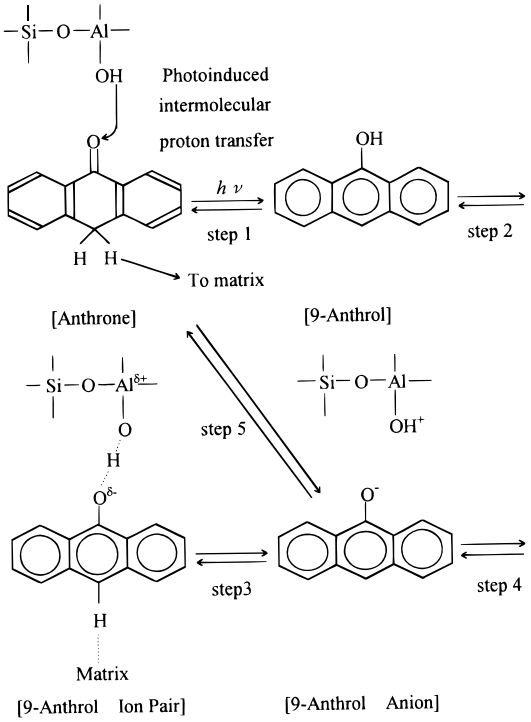


**Mechanism behind the Photoinduced Proton Transfer in the Xerogels.** Silica−alumina is a well-known and important acid catalyst.[38] Its catalytic properties strongly depend on the Si:Al ratio. The surface properties of the surrounding matrix around the mixed anthrone (and/or 9-anthrol) is an important factor in the photochromic behavior of the fluorescence spectra. The chemical reactions which occur on the silica−alumina surfaces are characterized by the Si:Al ratio. The conversion reactions show a maxima at a silica content of between 70 and 85%.[39] It was concluded that dehydrated alumina-in-silica contains only Brønsted acid sites comprised of tetracoordinate aluminum atoms. It is known that a proton linked to an oxygen interconnection of the $SiO_4$ and $AlO_4$ tetrahedral structure in silica−alumina exhibits a very strong acidic property. In the present gel systems, the surface chemical structure of the prepared gels may essentially be identical with that of the silica−alumina catalyst. Therefore, it can be concluded that a proton located at the Brønsted site directly denotes the proton to anthrone during the photoinduced proton-transfer reaction, resulting in the generation of 9-anthrol.

The results shown in Figure 2 indicate that the predominant species in the first stage is the hydrogen-bonded form and that in the xerogel state it is the complex between 9-anthrol and the −O−Si−O−Al−O− network. Analysis of the fluorescence lifetime (Table 1) and the results shown in Figure 6 show that the main fluorescent species existing in the gel before continuous irradiation is the complex form. Increase in the fluorescence intensity at 480 nm corresponds to the increase in the complex species. Based on these experimental results, the mechanism of the photoinduced proton-transfer reaction occurring for anthrone in the Si−Al matrixes is illustrated as in Scheme 2. The first step after the photoexcitation of anthrone is the generation of 9-anthrol, which was formed by the keto−enol isomerization from anthrone directly through the photoinduced proton transfer by the intermolecular proton transfer from the surface Brønsted acid site to anthrone (step 1). This step is quickly followed by the formation of the complex (step 2) which is responsible for the photochromic behavior in the fluorescence spectra of 9-anthrol encapsulated into the gels prepared by the sol−gel−xerogel transitions of silicon−aluminum mixed alkoxides. Further continuous irradiation on the gel systems decreased the fluorescence intensity at 480 nm. Some routes were found to be responsible for the decrease in fluorescence intensity. They are the route for the anionic form (step 3), and/or nonfluorescent species from the complex (step 4), and back reaction to anthrone (step 5) may be responsible for the decrease of the fluorescence intensity around 480 nm.

**Acknowledgment.** The authors would like to express thanks to Shin-Etsu Chemical Co. Ltd., for providing pure TEOS and Hitachi Chemical Co. Ltd. for donating the SAE used. This work was supported in part by a Grand-in-Aid on Priority-Area-Research "Photoreaction Dynamics" from the Ministry of Education, Science, Sports and Culture of Japan (Nos. 06239105 and 07228102). T.F. is much indebted to the Tokyo Ohka Foundation for their financial support.

## References and Notes

(1) de Mayo, P.; Johnston, L. J. *Preparative Chemistry Using Supported Reagent*; Academic Press: New York, 1987; p 61.

(2) Anpo, M.; Matsuura, T., Eds. *Photochemistry on Solid Surfaces*; Elsevier: Amsterdam, 1989.

(3) Dürr, H.; Bouas-Laurent, H., Eds. *Photochromism. Molecules and Systems*; Elsevier: Amsterdam, 1990.

(4) Ramamurthy, V., Ed. *Photochemistry in Organized & Constrained Media*, VCH: New York, 1991.

(5) Kaufman, V. R.; Avnir, D.; Rojanski, D.-P.; Huppert, D. *J. Non-Cryst. Solids* **1988**, *99*, 379.

(6) Matsui, K.; Matsuzuka, T.; Fujita, H. *J. Phys. Chem.* **1989**, *93*, 4991.

(7) Kaufman, V. R.; Levy, D.; Avnir, D. *J. Non-Cryst. Solids* **1986**, *82*, 103.

(8) Levy, D.; Avnir, D. *J. Phys. Chem.* **1988**, *92*, 4734.

(9) Preston, D.; Pouxviel, J.-C.; Novinson, T.; Kaska, W. C.; Dunn, B.; Zink, J. I. *J. Phys. Chem.* **1990**, *94*, 4167.

(10) Birks, J. B. *Photophysics of Aromatic Molecules*, Wiley-Interscience: London, 1970.

(11) Mataga, N.; Kubota, R. *Molecular Interactions and Electronic Spectra*, Marcel Dekker: New York, 1970.

(12) Smith, T. P.; Zaklika, K. A.; Thakur, K.; Walker, G.; Tominaga, C. K.; Barbara, P. *J. Phys. Chem.* **1991**, *95*, 10465 and special issue of *J. Phys. Chem.* **1991**, *95*, 10215−10524.

(13) Carter, T. P.; Gillispie, G. D.; Connolly, M. A. *J. Phys. Chem.* **1982**, *86*, 192.

(14) Marasinghe, P. A.; Gillispie, G. D. *Chem. Phys.* **1989**, *136*, 249.

(15) Inoue, H,; Hida, M.; Nakashima, N.; Yoshihara, K. *J. Phys. Chem.* **1982**, *86*, 3184.

(16) Barbara, P. F.; Walsh, P. K.; Brus, L. *J. Phys. Chem.* **1989**, *93*, 29.

(17) Graf, F.; Hong, H.-K.; Nazzal, A.; Haarer, D. *Chem. Phys. Lett.* **1978**, *59*, 217.

(18) Tani, T.; Namikawa, H.; Arai, K.; Makishima, A. *J. Appl. Phys.* **1985**, *58*, 3559. Makishima, A.; Tani, T. *J. Am. Ceram. Soc.* **1986**, *69*, C-72.

(19) Kümmerl, L.; Wolfrum, H.; Haarer, D. *J. Phys. Chem.* **1992**, *96*, 10688.

(20) Bansho, Y.; Nukada, K. *Bull. Chem. Soc. Jpn.* **1960**, *33*, 579.

(21) Baba, H.; Takemura, T. *Bull. Chem. Soc. Jpn.* **1964**, *37*, 1241. Baba, H.; Takemura, T. *Tetrahedron* **1968**, *24*, 4779. Takemura, T.; Baba, H. *Tetrahedron* **1968**, *24*, 5311.

(22) Löber, G. *Acta Chim. Hung.* **1964**, *40*, 9.

(23) Kanamaru, N.; Nagakura, S. *J. Am. Chem. Soc.* **1968**, *90*, 6905.

(24) Fujii, T.; Mishhima, S.; Tanaka, N.; Kawauchi, O.; Kodaira, K.; Nishikiori, H.; Kawai, Y. *Res. Chem. Intermed.*, in press.

(25) Avnir, D.; Kaufman, V.; Reisfeld, R. *J. Phys. Chem.* **1984**, *88*, 5956.

(26) Fujii, T.; Nishikiori, H. *Chem. Phys. Lett.* **1995**, *233*, 424. Nishikiori, H.; Fujii, T. *J. Phys. Chem. B* **1997**, *101*, 3680.

(27) Sakka, S. *Zoru-geru-houno no kagaku (Science of the sol−gel method)*; Agne Shofu Sha: Tokyo, 1988.

(28) Brinker, C. J.; Scherer, G. W. *Sol−Gel Science: the Physics and Chemistry of Sol−Gel Processing*; Academic Press: New York, 1990.

(29) Hench, L. L.; West, J. L. *Chem. Rev.* **1990**, *90*, 33.

(30) Avnir, D.; Braun, S.; Ottolenghi, M. *ACS Symp. Ser*. **1992**, *499*, 384.

(31) Dunn, B.; Zink, J. I. *J. Mater. Chem.* **1991**, *1*, 903. Zink, J. I.; Dunn, B. *J. Ceram. Soc. Jpn.* **1991**, *99*, 878.

(32) Fujii, T. *Trend Photochem. Photobiol*. **1994**, *4*, 243.

(33) Avnir, D. *Acc. Chem. Res*. **1995**, *28*, 328.

(34) Bauer, R. K.; Borenstein, R.; de Mayo, P.; Okada, K.; Rafalska, M.; Ware, W. R.; Wu, K. C. *J. Am. Chem. Soc*. **1982**, *104*, 4635.

(35) Bauer, R. K.; de Mayo, P.; Ware, W. R.; Wu, K. C. *J. Phys. Chem*. **1982**, *86*, 3781.

(36) Bauer, R. K.; de Mayo, P.; Natarajan, L. V.; Ware, W. R. *Can. J. Chem*. **1984**, *62*, 1279.

(37) Laidler, K. L. *Chemical Kinetics*, 3rd ed.; Harper & Row Publishers: New York, 1987.

(38) Benesi, H. J.; Winquist, B. H. *Advanced in Catalysis*, Academic Press: New York, 1978; p 78.

(39) Holm, V. C.; Clark, A. J. *J. Catal*. **1963**, *61*, 16.